Modeling energy storage and structural evolution during finite viscoplastic deformation of glassy polymers

Rui Xiao*
Institute of Soft Matter Mechanics, College of Mechanics and Materials, Hohai University, Nanjing, Jiangsu 210098, China

Gagik Ghazaryan
Department of Materials, ETH Zurich, 8093 Zurich, Switzerland and Laboratory for Biointerfaces, Empa, 9014 St. Gallen, Switzerland

Theo A. Tervoort
Department of Materials, ETH Zurich, 8093 Zurich, Switzerland

Thao D. Nguyen
Department of Mechanical Engineering, Johns Hopkins University, Baltimore, Maryland 21218, USA
(Received 3 January 2017; revised manuscript received 25 March 2017; published 6 June 2017)

The enthalpic response of amorphous polymers depends strongly on their thermal and deformation history. Annealing just below the glass transition temperature (T_g) causes a large endothermic overshoot of the isobaric heat capacity at T_g as measured by differential scanning calorimetry, while plastic deformation (cold work) can erase this overshoot and create an exothermic undershoot. This indicates that a strong coupling exists between the polymer structure, thermal response, and mechanical deformation. In this work, we apply a recently developed thermomechanical model for glassy polymers that couples structural evolution and viscoplastic deformation to investigate the effect of annealing and plastic deformation on the accumulation of stored energy during cold work and calorimetry measurements of heat flow. The thermomechanical model introduces the effective temperature as an additional state variable in a nonequilibrium thermodynamics setting to describe the structural evolution of the material. The results show that the model accurately describes the stress and enthalpy response of quenched and annealed polymers with different plastic predeformations. The model also shows that at 30% strain in uniaxial compression, 45% of the applied work is converted into stored energy, which is consistent with experimental data from literature.

DOI: 10.1103/PhysRevE.95.063001

I. INTRODUCTION

Glassy polymers have a frozen-in structure that is not in thermodynamic equilibrium and as a result their thermomechanical behavior depends on their thermal and mechanical history [1–3]. Annealing a polymer glass not too far below the glass-transition temperature (T_g) results in "physical aging", a slow, self-retarding approach to thermodynamic equilibrium that, among other things, manifests itself by an increase of the yield stress with annealing time as shown in Fig. 1(a) [1,4–6]. Conversely, it has been found that solid-state plastic deformation, such as from cold rolling or cold drawing, reverses the aging process (called "mechanical rejuvenation" [7]), thereby decreasing the yield strength and leading to a postyield stress drop [Fig. 1(a)]. This phenomenon is also called "intrinsic strain softening" [8,9], as opposed to "geometrical strain softening" that occurs only in tension when the increase in yield stress upon plastic deformation (strain hardening) is too small compared to the initial yield stress (Considère's construction) [2]. Calorimetric experiments show that physical aging and plastic deformation also produce significant changes in the internal energy as illustrated in Fig. 1(b). In a differential scanning calorimetry (DSC) test, physical aging produces an endothermic overshoot in the heat flow just above T_g that is attributed to enthalpy relaxation (see for example Hodge and Huvard [10]). The magnitude and shape of the overshoot and the temperature at which it occurs depend on the annealing time and temperature, as well as pretreatment conditions, such as the cooling rate prior to annealing, the heating rate, and the applied predeformation [1,10–14].

Moderate plastic deformation also produces a broad exothermic undershoot below T_g in the DSC measurement of heat flow [1,5,15–20], indicating that a significant portion of the work is converted to internal energy [Fig. 1(b)]. Rudnev [16] showed that the internal energy increases rapidly from 0–15% strain and levels off at 30–40% strain for a wide range of glassy polymers. At 40% strain, the stored energy ranges 15–50% of the applied work, depending on the polymer, and the remaining 50–85% of the applied work is dissipated as heat. This large increase in the internal energy to a new plateau indicates the occurrence of significant structural rearrangements away from equilibrium to a new metastable nonequillibrium state [17].

Enthalpy relaxation, and more broadly structural relaxation, has been explained successfully using the concept of a configurational temperature [21] or an equivalent order parameter [22,23] to describe the nonequilibrium thermodynamic state of amorphous materials cooled below the glass transition temperature [12,24]. The configurational temperature was introduced as an internal variable called "the fictive temperature"

*rxiao@hhu.edu.cn

 ©2017 American Physical Society

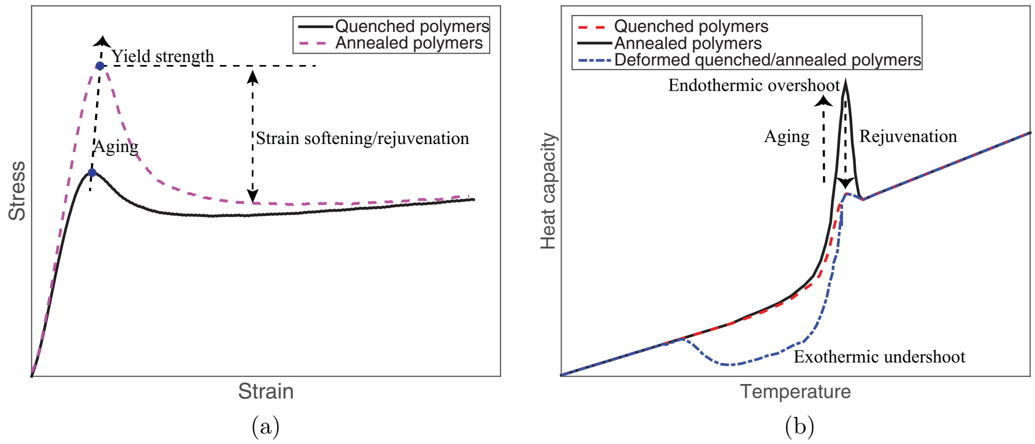

FIG. 1. Illustration of physical aging and mechanical rejuvenation in the: (a) stress response and (b) enthalpy response.

by Tool [21], then as a thermodynamic property called "the effective temperature" in the two-temperature thermodynamic theory for amorphous materials [25–28]. The two-temperature theory assumes that the thermodynamic properties of an amorphous glass can be described by two weakly interacting material subsystems, an equilibrium kinetic subsystem that represents the fast vibrational motions and a nonequilibrium configurational subsystem that represents the slow configurational rearrangements of the polymer segments. The effective temperature is defined as a thermodynamic conjugate to the configurational entropy. For an undeformed amorphous material being cooled below the glass transition, the effective temperature is typically higher than the experimental ("vibrational") temperature, because the frozen-in structure is more disordered than at thermodynamic equilibrium. During the physical aging process, the effective temperature then slowly evolves to converge with the experimental temperature until thermodynamic equilibrium is reached.

Langer and co-workers developed theoretical models for the plastic deformation of amorphous materials that relate the effective temperature to the density of shear transformation zones (STZ) [29–31]. By coupling structural evolution and plastic deformation, the STZ theories were able to describe the effect of aging and plastic deformation on the stress response and enthalpy. In simulations for the specific heat capacity, a more ordered initial structure, represented by a lower effective temperature, produced a larger endothermic overshoot at T_g, while a less ordered initial structure produced a greater exothermic undershoot below T_g [32]. Buckley and co-workers [33,34] and Xiao and Nguyen [35,36] also applied the effective temperature concept to model the viscoplastic deformation of amorphous polymers. The coupled thermomechanical model of Xiao and Nguyen [35] was able to describe accurately the experimentally measured effects of aging and plastic deformation on the yield stress, postyield strain-softening, and strain recovery upon unloading for different temperatures and strain rates [36].

The aim of this work is to investigate whether the thermomechanical Xiao and Nguyen model [35] that couples the evolution of the configurational structure to the viscoplastic deformation through the effective temperature, can also accurately describe the effect of aging and deformation on the enthalpy change and heat flow. To this extent, the model will be applied without additional parameters to simulate DSC experiments measuring the effects of aging time and plastic deformation on enthalpy relaxation and the stored energy due to cold work.

II. EXPERIMENTAL METHODS

The material used in this work is an acrylate-based random copolymer consisting of *tert*-butyl acrylate monomers and poly(ethylene glycol) dimethacrylate (PEGDMA) and di(ethylene glycol) dimethacrylate (DEGDMA) crosslinkers. The synthesis method has been described in detail in Xiao *et al.* [37] and Xiao and Nguyen [35]. Thermomechanical behavior of the thermosets was characterized using DSC, DMA, and uniaxial compression tests. To ensure that sequential thermal and mechanical measurements can be performed on a single sample, cylindrical specimens, with dimensions of 2.7 mm in diameter and 3.2 mm in height, were manufactured on a lathe.

In order to erase the thermomechanical history, the cylinders were heated in an oven at 80 °C for 30 min. Afterwards, the samples were quenched to 5 °C and stored at the same temperature in a refrigerator. The annealed specimens were obtained by placing the quenched cylinders in an oven at 35 °C for 24 h.

Dynamic mechanical analysis was performed on a DMA 861^e (Mettler Toledo, Greifensee, Switzerland) to obtain the relaxation spectrum of the material. The specimens were heated from 25 to 70 °C and subjected to a dynamic strain around 0.15%. Five different frequencies were chosen: 0.3, 1, 3, 10, and 30 Hz. The master curve was constructed by shifting the storage modulus at different temperatures with respect to a reference temperature of 70 °C, using time-temperature superposition.

Uniaxial compression was performed using an Instron 5864 static mechanical tester. For uniaxial precompression, the machined cylinders (2.7 mm in diameter and 3.2 mm in height) were compressed to different engineering strains (3, 8, 15, and 30%), followed by unloading the specimens to zero stress. Having measured the new dimensions, the deformed cylinders were subsequently compressed to a 30% engineering strain of the measured new length. All the compression experiments were performed at room temperature (around 22 °C). The precompressed tests used a constant loading speed of 0.192 mm/min, corresponding to an initial strain rate of 0.001/s. The reloading tests also used the engineering strain rate 0.001/s based on the measured new length. The actual loading speed was 0.192, 0.188, 0.175, and 0.146 mm/min for specimens with 3, 8, 15, and 30% precompressed strain respectively. The strain was calculated from the displacement between the clamps, corrected for the machine stiffness. To reduce the friction between samples and compression plates, silicon oil was sprayed on the compression plates. Visual inspection during the measurements of the plastically deformed samples confirmed that the applied deformations were to a good approximation homogeneous, and that barreling did not occur.

Thermal analysis was conducted using a differential scanning calorimeter (DSC 822^e, Mettler Toledo, Greifensee, Switzerland) calibrated with indium for temperature and enthalpy. DSC thermograms were recorded under N_2 purge at standard heating and cooling rates of 5 °C/min to reduce the effect of heat conduction. The DSC tests were performed on the undeformed quenched and annealed specimens, and annealed specimens with 3, 8, 15, and 30% precompressed strain.

III. COUPLED THERMOMECHANICAL THEORY

We have developed a thermomechanical model for the nonequilibrium behavior of amorphous polymers in our previous work [35]. The model was developed within a nonequilibrium thermodynamic framework, where the nonequilibrium state of the polymer is described by a set of internal variables for the viscous deformations and by the effective temperatures describing the nonequilibrium-configurational state. The evolutions of the viscous deformations and effective temperatures are described by the nonlinear Adam-Gibbs model of the dependence of the relaxation times on the temperature and effective temperatures [35,36]. In our previous work, we showed that the model can accurately capture the rate dependence and temperature dependence of the storage and loss moduli [35,37], stress response [35–37], coefficient of thermal expansion [37], and heat capacity [35].

Here, we briefly summarize the main assumptions and formulations. We first define the deformation gradient $\mathbf{F} = \partial\mathbf{x}/\partial\mathbf{X}$, mapping a material point $\mathbf{X}$ in the reference configuration to $\mathbf{x}$ in the current configuration. To describe the viscous deformation, the deformation gradient is decomposed to multiple pairs of elastic parts and viscous parts as $\mathbf{F} = \mathbf{F}^{\mathrm{e}}_j\mathbf{F}^{\mathrm{v}}_j, j = 1 \dots N$. The material systems are assumed to be composed of a kinetic subsystem and multiple configurational subsystems as

$$\Psi\left(\mathbf{C},\mathbf{C}^{\mathrm{e}}_j,T,T_{\mathrm{e}_i}\right) = \underbrace{e^k - T\eta^k}_{\Psi^k} + \sum_i^P \underbrace{e^c_i - T_{e_i}\eta^c_i}_{\Psi^c_i}, \quad (1)$$

where $\mathbf{C} = \mathbf{F}^{\mathrm{T}}\mathbf{F}$ is the right Cauchy deformation tensor, $\mathbf{C}^{\mathrm{e}}_j = \mathbf{F}^{\mathrm{eT}}_j\mathbf{F}^{\mathrm{e}}_j$ is the elastic right Cauchy deformation tensor, Ψ is the Helmholtz free energy density, e is the internal energy density, T is the temperature, η is the entropy, and T_{e_i} is the effective temperature of subsystem i. The superscripts k and c represent the kinetic subsystem and configurational subsystems respectively.

The Helmholtz free energy density is assumed to have the following form [35,38]:

$$\Psi^k = \sum_j^N \frac{(1-a)\mu^{\mathrm{neq}}_j}{2}\left[\mathrm{tr}\left(\overline{\mathbf{C}}^{\mathrm{e}}_j\right) - 3\right] + \frac{\kappa}{4}(J^2 - 2\ln J - 1) + c_{g0}(T - T_0) - c_{g0}T\ln\frac{T}{T_0} - \frac{c_{g1}}{2}(T-T_0)^2,$$

$$\Psi^c_i = \phi_i\frac{T_{e_i}}{T_0}\frac{\mu^{\mathrm{eq}}}{2}[\mathrm{tr}(\overline{\mathbf{C}}) - 3] + \phi_i\sum_j^N\frac{a\mu^{\mathrm{neq}}_j}{2}\left[\mathrm{tr}\left(\overline{\mathbf{C}}^{\mathrm{e}}_j\right) - 3\right] + \phi_i\Delta c_0(T_{e_i} - T_0) - \phi_i\Delta c_0 T_{e_i}\ln\frac{T_{e_i}}{T_2} - \phi_i\frac{\Delta c_1}{2}(T_{e_i} - T_2)^2, \quad (2)$$

where $J = \det\mathbf{F}$, $\overline{\mathbf{C}} = J^{-2/3}\mathbf{C}$, $\overline{\mathbf{C}}^{\mathrm{e}}_j = J^{\mathrm{e}-2/3}_j\mathbf{C}^{\mathrm{e}}_j$, μ^{eq} is the equilibrium shear modulus, μ^{neq}_j are the nonequilibrium shear moduli of the stress relaxation spectrum, κ is the bulk modulus, c_{g0} and c_{g1} are coefficients of the heat capacity of the kinetic subsystem, Δc_0 and Δc_1 are the coefficients of the heat capacity of the configurational subsystems, ϕ_i characterizes the structural relaxation spectrum with $\sum_i^P \phi_i = 1$, T_0 is the reference temperature, T_2 is the Kauzmann temperature, and a is the fractional parameter of the total contribution of the inelastic internal energy to the configurational subsystems. All parameters and their values are listed in Table I.

The Cauchy stress tensor can be calculated as $\sigma = 2\frac{1}{J}\mathbf{F}\frac{\partial\Psi}{\partial\mathbf{C}}\mathbf{F}^{\mathrm{T}}$. The kinetic entropy can be calculated as $\eta^k = -\frac{\partial\Psi}{\partial T}$, and the configurational entropy can be calculated as $\eta^c_i = -\frac{\partial\Psi}{\partial T_{e_i}}$, which give

$$\sigma = \sum_i^P \underbrace{\frac{1}{J}\phi_i\frac{T_{e_i}}{T_0}\mu^{\mathrm{eq}}\left(\overline{\mathbf{b}} - \frac{1}{3}\mathrm{tr}(\overline{\mathbf{b}})\mathbf{1}\right)}_{\mathbf{s}^{\mathrm{eq}}_i} + \sum_j^N \underbrace{\frac{1}{J}\mu^{\mathrm{neq}}_j\left(\overline{\mathbf{b}}^{\mathrm{e}}_j - \frac{1}{3}\mathrm{tr}\left(\overline{\mathbf{b}}^{\mathrm{e}}_j\right)\mathbf{1}\right)}_{\mathbf{s}^{\mathrm{neq}}_j} + \underbrace{\frac{1}{2J}\kappa(J^2-1)\mathbf{1}}_{p},$$

$$\eta^k = c_{g0}\ln\frac{T}{T_0} + c_{g1}(T - T_0),$$

$$\eta^c_i(T_{e_i},\mathbf{C}) = \phi_i\Delta c_0\ln\frac{T_{e_i}}{T_2} + \phi_i\Delta c_1(T_{e_i} - T_2) - \frac{\phi_i}{T_0}\frac{\mu^{eq}}{2}[\mathrm{tr}(\overline{\mathbf{C}}) - 3]. \quad (3)$$

TABLE I. Parameters of the thermomechanical model.

Parameter	Value	Physical significance
μ^{eq} (MPa)	1.57	equilibrium shear modulus at $T_0 = 343$ K
κ (MPa)	1333.3	bulk modulus
Q_s/s_y (K/MPa)	90.0	activation parameter for viscous flow
B (J/g)	500.0	thermal activation energy
T_2 (K)	277.25	Kauzmann temperature
T_g (K)	316	glass transition temperature
T_0 (K)	343	reference temperature
c_{g0} [J/(cm^{3}K)]	0.2844	coefficient of heat capacity of kinetic subsystem
c_{g1} [J/(cm^{3}K^2)]	0.0036	coefficient of heat capacity of kinetic subsystem
Δc_0 [J/(cm^{3}K)]	0.8693	coefficient of excess heat capacity of configurational subsystems
Δc_1 [J/(cm^{3}K^2)]	−0.0017	coefficient of excess heat capacity of configurational subsystems
a_0	0.8	ratio of the fractional parameter
a_1	500	decay rate of the fractional parameter
T_e^{∞} (K)	316	equilibrium effective temperature
k [W/(m K)]	0.1	thermal conductivity
h_1 [W/(m^2 K)]	85	convection coefficient between polymer and pan
h_2 [W/(m^2 K)]	40	convection coefficient between polymer and air

The total internal energy density of the the polymer system can be represented as

$$e = \underbrace{\sum_j^N \frac{\mu_j^{\text{neq}}}{2}\left[\text{tr}\left(\overline{\mathbf{C}}_j^{\text{e}}\right) - 3\right] + \frac{\kappa}{4}(J^2 - 2\ln J - 1)}_{e_M} + \underbrace{c_{g0}(T - T_0) + c_{g1}\left(T^2 - T_0^2\right)/2}_{e_T}$$
$$+ \underbrace{\sum_i^P \left[\Delta c_0 \phi_i (T_{e_i} - T_0) + \Delta c_1 \phi_i \left(T_{e_i}^2 - T_2^2\right)/2\right]}_{e_{T_e}}. \tag{4}$$

Following the discussion in Xiao and Nguyen [35], the following evolution equation is applied to describe the evolution of viscous deformation tensor $\mathbf{F}_j^{\text{v}}$:

$$\mathbf{D}_j^{\text{v}} = \frac{\mathbf{M}_j}{2\upsilon_j}, \quad \mathbf{M}_j = \sum_i^P 2\frac{T}{T_{e_i}}\mathbf{C}_j^{\text{e}}\frac{\partial \Psi_i^c}{\partial \mathbf{C}_j^{\text{e}}} + 2\mathbf{C}_j^{\text{e}}\frac{\partial \Psi^k}{\partial \mathbf{C}_j^{\text{e}}} = \sum_i^P \phi_i\left[1 + a\left(\frac{T}{T_{e_i}} - 1\right)\right]\underbrace{\mu_j^{\text{neq}}\left(\overline{\mathbf{C}}_j^{\text{e}} - \frac{1}{3}\text{tr}\left(\overline{\mathbf{C}}_j^{\text{e}}\right)\mathbf{I}\right)}_{\mathbf{M}_j^{\text{e}}}, \tag{5}$$

where $\mathbf{D}_j^{\text{v}} = \frac{1}{2}[\dot{\mathbf{F}}_j^{\text{v}}\mathbf{F}_j^{\text{v-1}} + (\dot{\mathbf{F}}_j^{\text{v}}\mathbf{F}_j^{\text{v-1}})^{\text{T}}]$, $\mathbf{M}_j$ is the flow stress tensor, which reduces to the Mandel stress tensor $\mathbf{M}_j^{\text{e}}$ at structural equilibrium when $T_{e_i} = T$. The υ_j is the viscosity of each relaxation process. The stress relaxation time is defined as $\tau_{S_j} = \upsilon_j/\mu_j^{\text{neq}}$.

The governing equation for the effective temperatures can be written as [35,36]

$$\dot{T}_{e_i} = \frac{T - T_{e_i}}{\tau_{R_i}} + \frac{a}{\Delta c_0 + \Delta c_1 T_{e_i}}\sum_j^N \mathbf{M}_j^{\text{e}} : \mathbf{D}_j^{\text{v}} + \frac{J\mathbf{s}_i^{eq} : \mathbf{D}}{(\Delta c_0 + \Delta c_1 T_{e_i})\phi_i}, \tag{6}$$

where $\mathbf{D} = \frac{1}{2}(\dot{\mathbf{F}}\mathbf{F}^{-1} + \mathbf{F}^{\text{-T}}\dot{\mathbf{F}}^{\text{T}})$ is the rate-of-deformation tensor and τ_{R_i} is the structural relaxation time. The first term on the right side describes the ordering effect of physical aging, while the second term on the right side represents the disordering effect of plastic work. The third term represents the latent heat term caused by the thermomechanical coupling. In the above formulation, we have ignored the diffusion of effective temperatures, which may play an important role in the localization of plastic deformation [39].

The governing equation for the temperature can be written as

$$(c_{g0} + c_{g1}T)\dot{T} + \sum_i^P \phi_i(\Delta c_0 + \Delta c_1 T_{e_i})\dot{T}_{e_i} = -\nabla_{\mathbf{X}} \cdot \mathbf{Q} + \sum_j^N \mathbf{M}_j^{\text{e}} : \mathbf{D}_j^{\text{v}} + J\sum_i^P \mathbf{s}_i^{eq} : \mathbf{D}. \tag{7}$$

The Fourier conduction law is used to describe heat flow in the spatial configuration, $\mathbf{q} = -k\nabla_{\mathbf{x}}T$, where k are thermal conductivity and $\mathbf{q}$ is the heat flow in the spatial configuration. The conduction law can also be written in the reference configuration as $\mathbf{Q} = -k\mathbf{C}^{-1}\nabla_{\mathbf{X}}T$.

We applied the Adam-Gibbs theory to describe the dependence of stress and structural relaxation time on temperature and nonequilibrium structure through the effective temperature. The Eyring stress-activation theory for viscoplastic flow is used to describe the dependence of the stress relaxation time on the magnitude of the flow stress,

$$\tau_{S_j} = \tau_{S_j}^g \exp\left(\frac{B}{T\sum_i^P \eta_i^c(T_{e_i},\mathbf{C})} - \frac{B}{T\sum_i^P \eta_i^c(T_g,\mathbf{I})}\right)\frac{Q_s s}{T s_y}\left[\sinh\left(\frac{Q_s s}{T s_y}\right)\right]^{-1},$$
$$\tau_{R_i} = \tau_{R_i}^g \exp\left(\frac{B}{T\sum_i^P \eta_i^c(T_{e_i},\mathbf{C})} - \frac{B}{T\sum_i^P \eta_i^c(T_g,\mathbf{I})}\right). \tag{8}$$

Here, B is thermal energy, Q_s is the activation volume, s_y is the yield strength, $s = \sqrt{\frac{1}{2}\sum_j^N \mathbf{M}_j : \sum_j^N \mathbf{M}_j}$ is the flow stress, and $\tau_{S_j}^g$ and $\tau_{R_i}^g$ are the characteristic stress and structural relaxation time at T_g.

In Xiao and Nguyen [35,36], the fractional parameter a was assumed to be a constant value. As a result, the stress response continued to slowly decay with strain after the initial postyield stress drop. This did not agree with experiments, which shows a draw stress after yield followed by strain hardening with further increases in strain. To capture these phenomena and improve the agreement with experiments, we assume the following sigmoidal form of the fractional parameter:

$$a = a_0\left(1 - \frac{1}{1+\exp\left[-a_1\left(\frac{T_e}{T_e^\infty} - 1\right)\right]}\right), \tag{9}$$

where $0 \leqslant a_0 \leqslant 1$, $a_1 \geqslant 0$ is a constant, $T_e = \sum_i^P \phi_i T_{e_i}$ is the weighted average of the effective temperature, and T_e^∞ is the long-time effective temperature. This equation implies a decrease of rejuvenation effect when T_e approaches T_e^∞ and the deformed material reaches a more disordered, metastable nonequilibrium state. The logistic function for the fractional parameter automatically satisfies the condition that $0 \leqslant a \leqslant 1$.

IV. FINITE ELEMENT SIMULATION

The above thermomechanical theory was implemented into the finite element program Tahoe [40] and applied to numerically simulate the DSC experiments. The coupled thermomechanical boundary value problems were solved using a staggered scheme, where the thermal diffusion problem was solved first for the temperature field. The temperature field was used to solve the mechanical equilibrium equations for the displacement field and stress response. The displacement field was applied to update the configuration to solve for the updated temperature field. This staggered solution scheme was repeated at each time step until convergence was achieved for both the thermal and mechanical fields.

We developed an axisymmetric model to simulate the thermal diffusion and uniaxial compression of the cylindrical specimens. Figure 2 shows a schematic of the finite element model. Bilinear quadrilateral elements were used to discretize the geometry. The normal displacement components were fixed at the axis of symmetry and at the bottom of the specimen, such that $u_x(AB) = 0$ $u_y(AC) = 0$ and displacements were applied to the top surface, $u_y(BD) = u(t)$, where $u(t)$ is the applied displacements in the uniaxial compression tests. The remainder of the surfaces were assumed to be traction free. For the thermal diffusion problem, we assumed a convection boundary condition at the surface AC to describe the resistance to heat transfer between the specimen and the DSC steel pan, $\mathbf{q} = h_1(T - T_{DSC})\mathbf{n}$, where $\mathbf{n}$ is the normal direction of the surface and h_1 is the heat transfer coefficient. We also assumed a convection boundary condition at the surfaces CD and BD with the air, $\mathbf{q} = h_2(T - T_{DSC})\mathbf{n}$, where h_2 is the coefficient for natural convection and $T_{DSC}(t)$ is the temperature in the DSC tests.

Thermal diffusion causes the specimen to exhibit an inhomogeneous displacement and temperature field. To compare to experimental measurements of the macroscopic stress and heat flux, we obtain the nominal stress from finite element results through

$$\bar{\sigma} = F_y/A_t, \tag{10}$$

where F_y is the vertical component of the reaction force acting on the surface BD and A_t is the area computed at BD. In the first loading cycle, A_t was the area of the undeformed specimen. In the second loading cycle, A_t was the area of the predeformed unloaded specimen. Thus, $\bar{\sigma}$ is the nominal stress (engineering stress). The macroscopic specific heat flux can be calculated from Eq. (7) as

$$\overline{Q} = \frac{1}{\rho V}\int\left((c_{g0} + c_{g1}T)\dot{T} + \sum_i^P \phi_i(\Delta c_0 + \Delta c_1 T_{e_i})\dot{T}_{e_i} - \sum_j^N \mathbf{M}_j^{\mathrm{e}} : \mathbf{D}_j^{\mathrm{v}} - J\sum_i^P \mathbf{s}_i^{eq} : \mathbf{D}\right)dV, \tag{11}$$

where $\rho = 1.2$ g/cm^3 is the density of the polymer. The unit of $\overline{Q}$ is W/g.

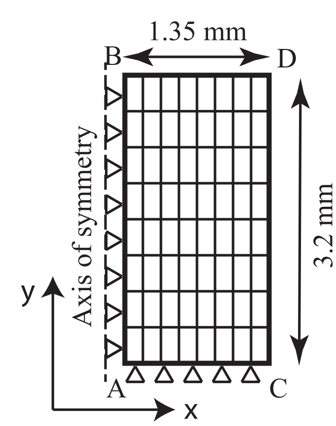

FIG. 2. An axisymmetric finite element mesh of the cylindrical specimens.

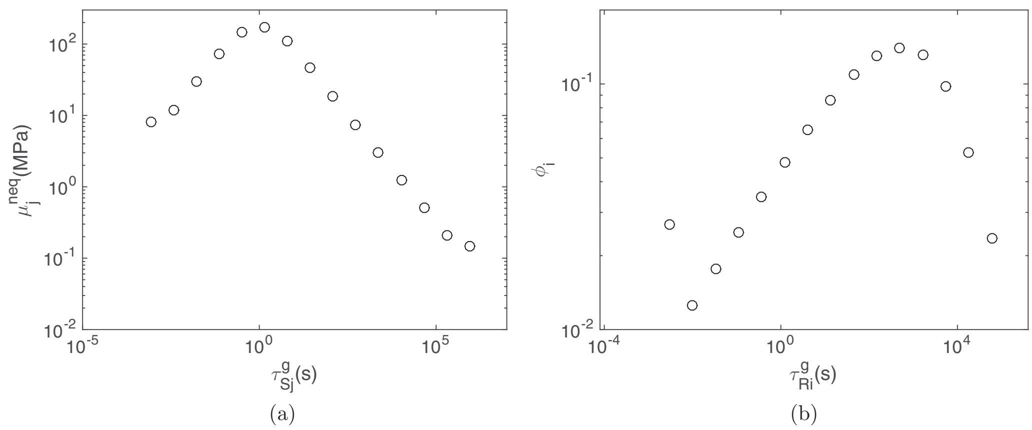

FIG. 3. The (a) stress relaxation spectrum and (b) structural relaxation spectrum.

V. PARAMETER DETERMINATION

All the parameters and their physical meaning are shown in Table I. The stress and structural relaxation spectra are plotted in Fig. 3. The onset of the glass transition is defined by the intersection of two lines fitted to the glassy plateau and the glass transition region of the storage modulus and occurs at $T_g = 43\,^\circ$C. The parameters μ^{eq}, κ, and stress relaxation spectrum $(\mu_j^{neq}, \tau^g_{S_j})$ were fit to the master curve of the storage modulus [Fig. 4(a)] obtained from the dynamic temperature and frequency sweep tests for a reference temperature $T_0 = 70\,^\circ$C using the method previously described in Xiao *et al.* [37] and Xiao and Nguyen [35]. The model assumed a constant glassy modulus for frequencies greater than 10^7 Hz, by neglecting the effects of relaxation times smaller than 10^{-3} s at T_g. However, the experimental measurements showed that the glassy modulus continued to increase because of these faster relaxation mechanisms.

The parameters B and T_2 were fit to the shift factor used to construct the master curve. The experimentally measured shift factor exhibited an Arrhenius temperature dependence for temperatures $T < 47\,^\circ$C, where the shift factor decreased linearly with $1/T$. The shift factor exhibited a steeper decay with $1/T$ for $T = 47$–$70\,^\circ$C in a manner that is typical of the equilibrium behavior of polymers. For simplicity, we fit the parameters B and T_2 to the temperature range 47–70 °C, for which the material can be assumed to be in structural equilibrium and $T_{ei} = T$. The parameters for the stress-relaxation spectrum and temperature dependence of the relaxation times were validated by applying the model to evaluate the temperature dependence of the storage and loss moduli at 40–70 °C, 0.15% dynamic strain, and 1 Hz [Figs. 4(c) and 4(d)]. The model was able to accurately predict the experimentally measured temperature dependence of the storage and loss moduli particular for $T > T_g$. The discrepancy between the measured and simulated loss modulus below T_g likely occurred because the model did not capture the relaxation behavior at high frequencies and, by extension, low temperatures [Fig. 4(a)].

The heat capacity of kinetic subsystem c_{g0} and c_{g1} were obtained from a linear fit of the DSC scan of the quenched specimen from 0 to 10 °C, while the heat capacity of the total system was obtained from a linear fit of the DSC scan of the quenched specimen from 60 to 70 °C. The difference of the two fits gave the values of the heat capacity of the configurational subsystems Δc_0 and Δc_1. To obtain the structural spectrum $(\tau^g_{R_i}, \phi_i)$, the Kohlrausch-Williams-Watts (KWW) model with two parameters signifying the characteristic structural relaxation time and breadth of the relaxation spectrum were used to fit the DSC scan of the quenched undeformed specimen as described in Xiao and Nguyen [35]. The convection coefficient h_1 was chosen as the same value in Arruda *et al.* [41]. The parameters Q_s/s_y, a_0, a_1, and T_e^∞ were obtained by fitting the experimentally measured stress response of the annealed specimen compressed to 30% engineering strain.

VI. RESULTS AND DISCUSSIONS

We first applied the model to describe the stress response of annealed and quenched specimens subjected to uniaxial compression at 0.001/s strain rate. To simulate the stress response of the annealed material, the temperature was decreased linearly from 70 to 35 °C at 10 °C/min and held at the same temperature for 24 h. The temperature was then ramped up to 22 °C (room temperature) at 10 °C/min and held for 30 min. For the quenched material, the temperature was decreased from 70 to 22 °C at 10 °C/min. The temperature was then held for 30 min. After the above-mentioned thermal histories, the displacement boundary condition was applied. Only the data from the annealed specimen with no predeformation were used to fit the model parameters. As shown in Fig. 5(a), the model was able to accurately capture the difference in the stress response of quenched and annealed specimens. The annealed specimen showed a larger yield stress and postyield stress drop because annealing allowed the material to attain a more ordered configurational structure, which had a lower molecular mobility and higher resistance to plastic flow. Both simulation and experimental results showed that the steady-state flow stress was independent of the thermal history. Mechanical deformation had a significant influence on the stress response. The yield strength decreased with increasing the prestrain (Fig. 6). The yield strength of annealed specimens with 3% prestrain was close to that of the undeformed annealed specimens, which suggested that little rejuvenation occurred prior to yield. The postyield stress drop nearly vanished

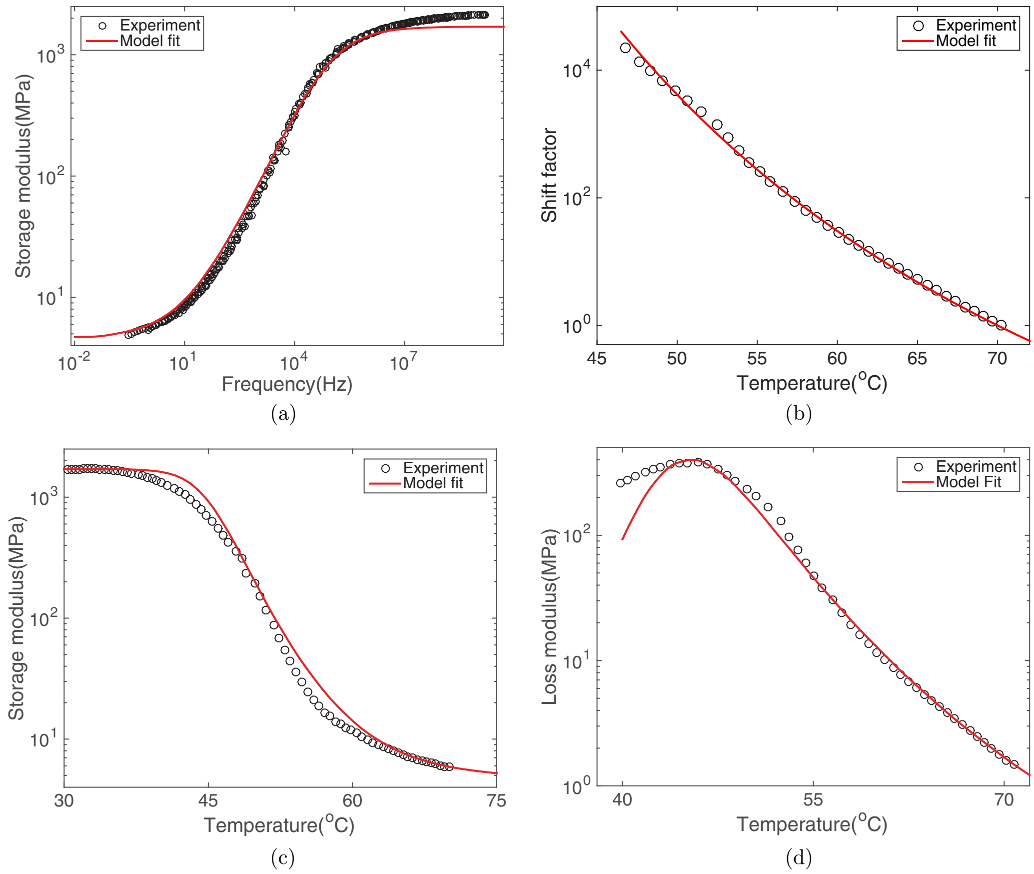

FIG. 4. Experimental data and model fit of the dynamic thermomechanical properties showing: (a) the master curve of the storage modulus at 70 °C, (b) the temperature-dependent shift factor, (c) the storage modulus at 1 Hz frequency and (d) the loss modulus at 1 Hz frequency.

for 30% precompression, which suggested that the effect of mechanical rejuvenation was near saturation and the large plastic deformation produced a metastable nonequilibrium structure.

The model was then applied to study the enthalpy response of annealed and quenched specimens subjected to different precompression strains. After simulating the first compression loading, the stress was decreased to zero in 10 sec and kept stress free in the following simulation. The temperature was then decreased from 22 °C to −10 °C at 5 °C/min and held at −10 °C for 5 min before ramping to 70 °C at 5 °C/min. Figure 7 shows good qualitative agreement between the measured and simulated heat flow [Eq. (11)] of the quenched and annealed specimens subjected to 0% prestrain. Recall that only the DSC curve of the quenched specimen well above and well below T_g was used to fit the heat capacity parameters. The annealed specimen exhibited a significantly larger overshoot above T_g than the quenched specimen caused by the slow approach to equilibrium of the specimen during annealing. Figures 7(b) and 7(c) show the effect of prestrain on the heat flow curves. The overshoot decreased with increasing prestrain and vanished entirely when compressed beyond 15% strain. An exothermic undershoot developed in the heat flow for prestrains between 15% and 30% in both the experimental and modeling results, caused by the release of the stored energy during the heating process. Though the model can capture the main characteristics of experimental observations, the exothermic undershoot peak appeared slightly below T_g^{onset}, which was 9 °C lower than measured in experiments. Moreover, the magnitude of the exothermic undershoot was larger than measured in experiments at 30% precompression. Despite these differences, the model accurately described the increase in the magnitude of the exothermic undershoot with prestrain, the decrease in the endothermic overshoot with prestrain, and the temperature of the overshoot. Moreover, both the model and experiments showed that the DSC curves were nearly identical for annealed and quenched specimens subjected up to 30% prestrain. This indicated that the large plastic deformation removed the effects of thermal history resulting in a rejuvenated, metastable nonequilibrium state.

The heating rate will have an effect on the shape (magnitude and width) of the endothermic overshoot and the temperature at which the peak occurs. Enthalpy recovery shifts to higher temperatures with higher heating rate, and the magnitude of the enthalpy overshoot first increases then decreases with heating rate (Fig. 8). The rate dependence occurs because of heat conduction, with its characteristic size-dependent diffusion time, and structural relaxation, with its characteristic relaxation time. A higher heating rate means less time for structural relaxation, which can result in a higher but narrower enthalpy overshoot. A higher heating rate also induces a larger temperature gradient, which leads to a smaller enthalpy overshoot. To quantify the effect of heat conduction in the experiments, we performed preliminary DSC measurements

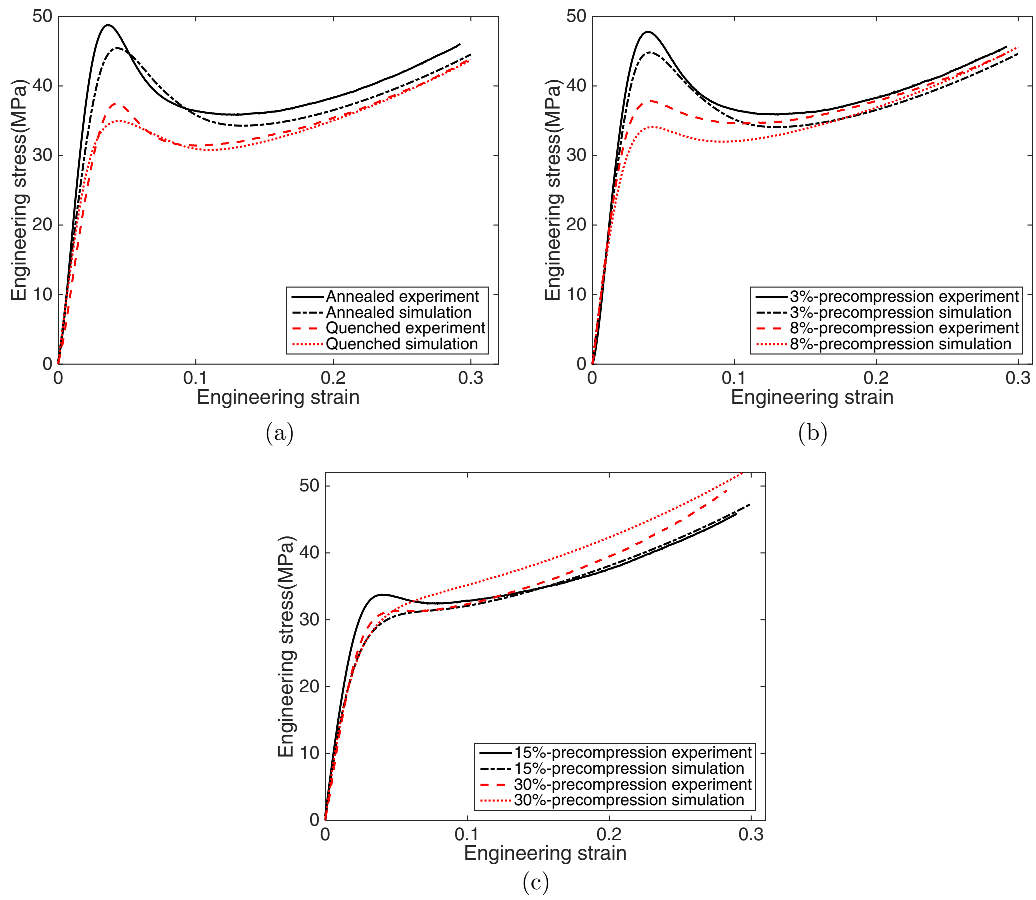

FIG. 5. Comparing the experimentaly measured and model prediction of the stress response of (a) annealed and quenched specimen, (b) annealed specimen with 3% and 8% precompression strain and (c) annealed specimen with 15% and 30% precompression strain.

on PS and PCL specimens of similar size for heating rates ranging from 1 to 10 °C/min and found little difference in the heat flow curves for 5 and 3 °C/min, which signifies that the effect of heat conduction was likely small for heating rates 5 °C/min and below. We chose 5 °C/min for

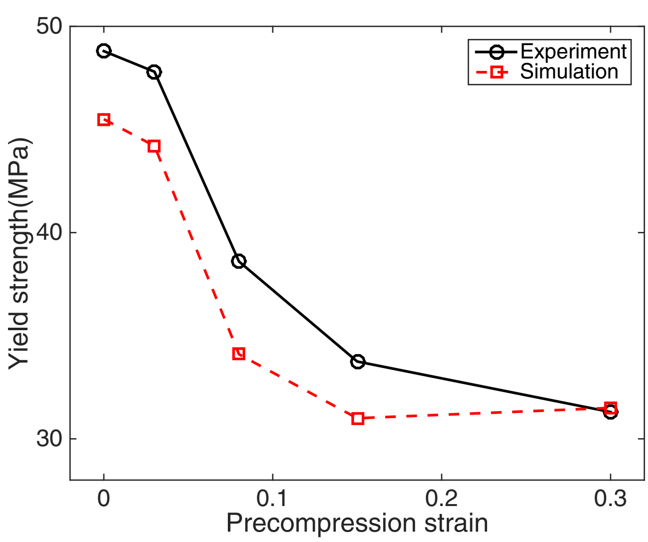

FIG. 6. Yield strength as a function of the precompression strain.

its shorter experimental time. The effects of heat transfer and structural relaxation were both captured by the finite element simulations, which solved the coupled heat transfer and mechanics problems. Preliminary simulations also showed that the cooling rate during annealing had a small effect on the heat flow curves.

Next, we investigated the change in energy of the quenched and annealed specimens during deformation. From Eq. (4), the internal energy consists of three components: the mechanical component e_M from inelastic and volumetric deformation, the thermal component e_T caused by a temperature change with respect to the reference temperature, and the structural component e_{T_e} caused by structural evolution from the initial configurational state, which does not appear in the classical equilibrium thermodynamics theories. The specific internal energy change was evaluated as $\Delta e = [e(\epsilon(t)) - e(\epsilon = 0)]/\rho$. The internal energy increment and the mechanical work of the quenched and annealed polymers are plotted in Figs. 9(a) and 9(b) during deformation to 30% strain at 22 °C and strain rate 0.001/s. Though the increase in the energy with deformation differed in magnitude between the annealed and quenched specimens, both specimens exhibited the same trends. The thermal component was the smallest because the temperature increased only slightly by 0.4 °C during deformation to 30% strain. The temperature e_T did not increase until the material yielded at 5% strain. The e_T increased rapidly between 5%

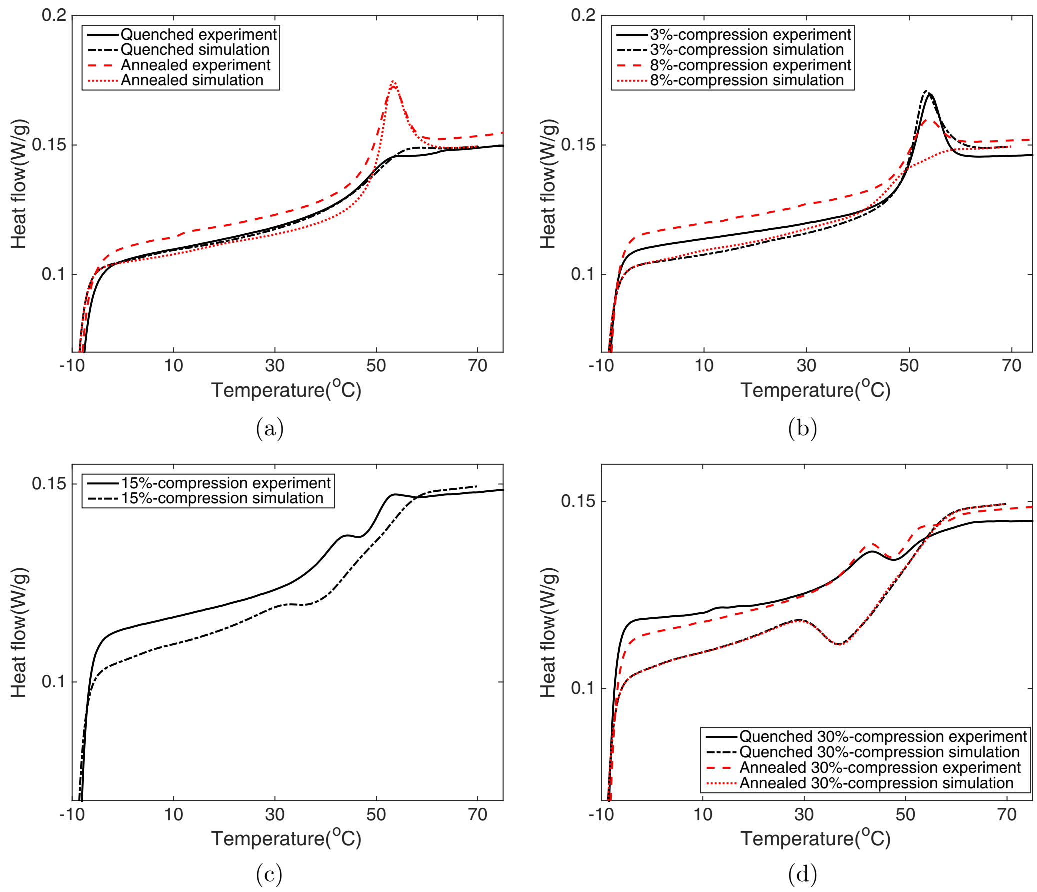

FIG. 7. Comparison the measured and model prediction of the DSC response for (a) annealed and quenched undeformed specimen, (b) annealed specimens with 3% and 8% compression strain, (c) annealed specimens with 15% compression strain, (d) annealed and quenched specimens with 30% compression strain.

and 15% strain then more slowly at higher strains. The energy from structural rearrangements e_{T_e} followed the same trend as e_T, increasing first rapidly from 5% to 15% strain before leveling off to a much slower increase at higher strains. This

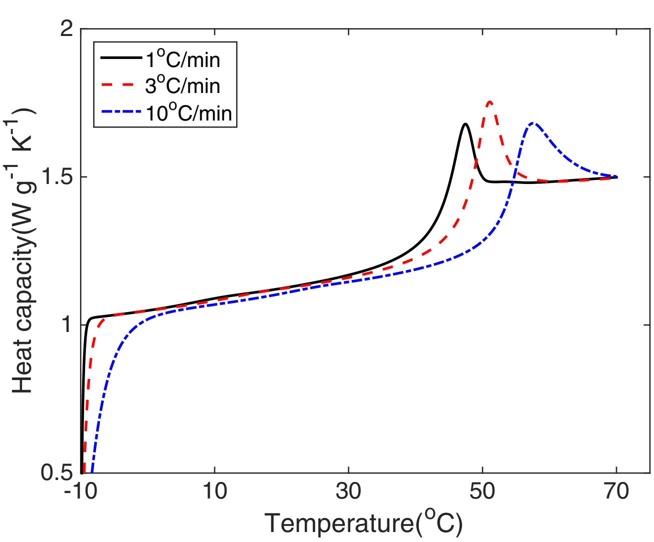

FIG. 8. Simulation results of the influence of heating rate on the enthalpy relaxation.

is consistent with the experimental observations that polymers showed almost identical mechanical response after 20% strain. The mechanical component also increased with strain, which explains the appearance of a larger exothermic undershoot for polymers with larger deformation [1].

We also plotted the ratio of $\Delta e_M + \Delta e_{T_e}$ and the work W as shown in Fig. 9(c). The remaining fraction Δe_T is the heat generation caused by plastic deformation. At the beginning of the deformation, this value was close to 1 and gradually decreased to around 45%. Figure 9(c) also plots experimental data for polycarbonate (PC), atactic polyethylene-terephthalate (α-PET), and polyimide based on benzophenon tetracarboxylic acid dianhydride and 4,4'-diaminodiphenyl ether (PI-BD) obtained from the deformation calorimetry measurements of Salamatina *et al.* [42], as well as experimental data for polyimid PI [(poly-benzo phenon)-imid] (PIM), polymethylmethacrylate (PMMA), and polystyrene (PS) obtained from Oleinik *et al.* [19]. The simulation predictions, which were obtained using parameters determined for the acrylate copolymer, showed good agreement with the data measured for the different glassy polymers, though the measured results of PIM and PI-BD were higher than simulation. We also want to emphasize that during the unloading and cooling process, some amount of the "stored" energy is further dissipated. Thus, only part of the "stored" energy during the deformation can be measured during the DSC tests. Figure 9(d) plots the ratio of

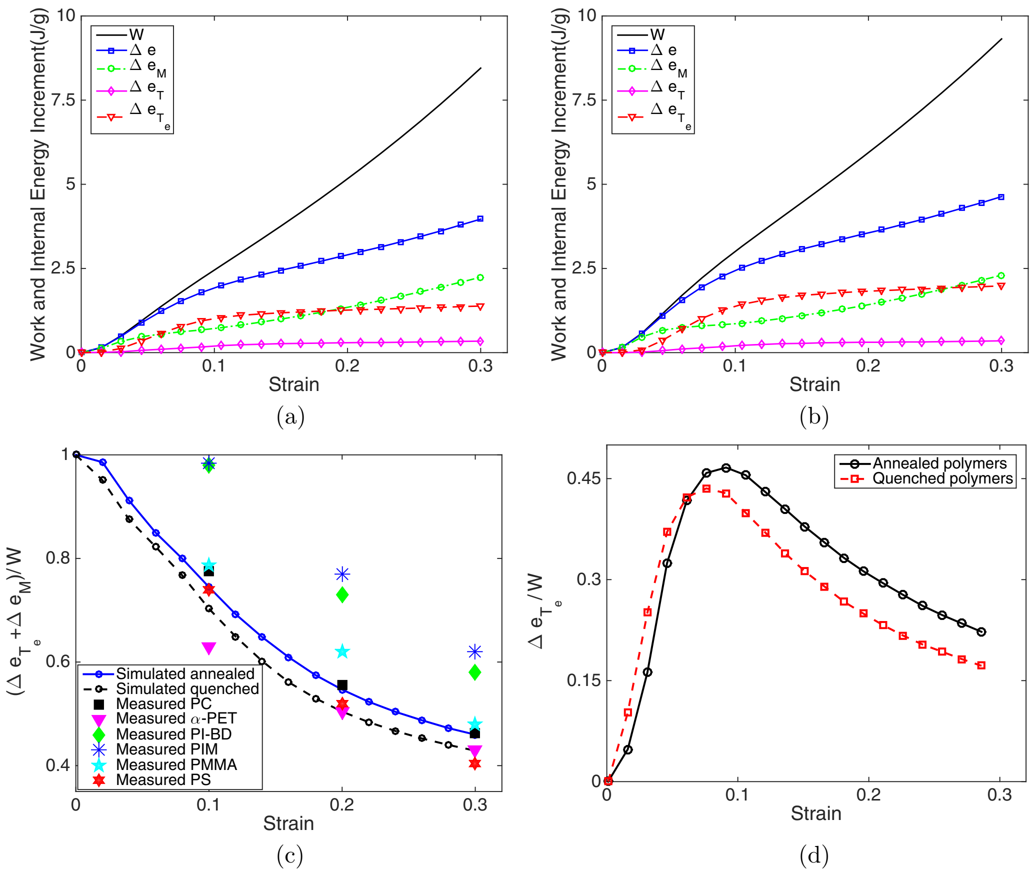

FIG. 9. The work and increment of the internal energy during the deformation at room temperature for (a) quenched specimen and (b) annealed specimen. (c) Comparision of the ratio between the stored energy and applied work predicted by the model and measured for different glassy polymers. (d) The ratio between the structural internal energy and applied work for the annealed and quenched materials.

structural internal energy change Δe_{T_e} and the applied work W. As shown, this value first increased to a peak value and then gradually decreased as the polymer was further deformed. The peak value reached as high as 45%, suggesting that a large fraction of the applied work is "stored" in the configurational subsystems during the early stage of the deformation.

Finally, in order to investigate the discrepancy of the occurrence of the undershoot, we performed a parameter study to investigate the influence of relaxation spectra on the undershoot of enthalpy response of annealed specimens deformed to 30% strain. Figures 10(a) and 10(b) plot the influence of characteristic relaxation time on the enthalpy response. As shown, increasing the stress-relaxation time shifted the undershoot to higher temperatures and also increased the magnitude of the undershoot, while increasing the structural relaxation time had little effect on the location of undershoot but significantly decreased the magnitude of the undershoot. A larger stress-relaxation time and a smaller structural-relaxation time produced a larger flow stress during the compression, which allowed more internal energy stored and released later during the heating process. The breadth of the stress and structural-relaxation spectra can be represented as a single parameter α in the analogous continuous fractional derivative model used to determine the discrete stress relaxation spectrum, and β in the analogous KWW model used to determine the discrete structural relaxation spectrum, as described in Xiao *et al.* [37]. The discrete distribution of relaxation processes of the spectra of different α and β is plotted in Figs 10(c) and 10(e). As shown in Fig. 10(d), the breadth of the stress-relaxation spectrum does not influence the location of the undershoot. However, a narrower stress-relaxation spectrum leads to a much smaller undershoot due to faster stress-relaxation rate and more dissipation during the unloading and cooling process. In comparison, a narrower structural relaxation spectrum reduced the magnitude of the undershoot and shifted it to higher temperatures, though the effect saturates at T_g. The experiments showed that the exothermic undershoot occurred at much higher temperatures. The discrepancy may also be caused by the modeling assumption that the structural relaxation time τ_{R_i} is independent of the flow stress [43]. The model also ignored the effect of molecular orientation at large strain.

VII. CONCLUSION

Describing the finite thermomechanical deformation response of glassy polymers remains a challenging topic in mechanics and physics. This is because the material exhibits measurable structural evolution (as evidenced by time-dependent processes such as enthalpy relaxation, volume relaxation, physical aging, and mechanical rejuvenation), whereas no corresponding ordered microstructure or microstructural

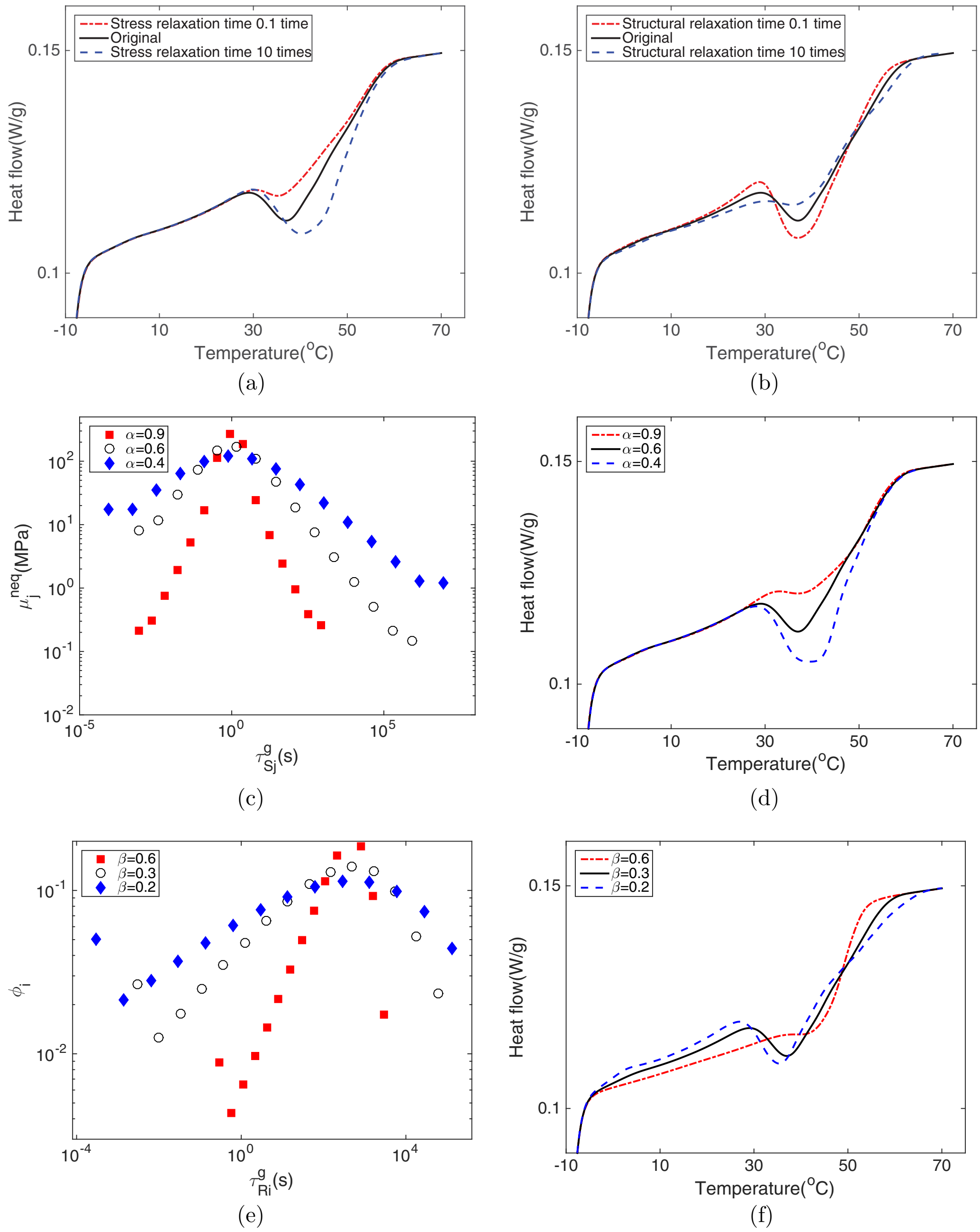

FIG. 10. Influence of (a) characteristic stress relaxation time, (b) characteristic structural relaxation time on heat flow, (c) the shape of stress relaxation spectrum of different α, (d) influence of the breadth of stress relaxation spectrum on heat flow, (e) the shape of structural relaxation spectrum of different β, (f) influence of the breadth of structural relaxation spectrum on heat flow.

defect can be clearly identified. The nonequilibrium structure depends on a large number of factors, including the cooling or heating rate, annealing time, temperature, plastic deformation, and stress. At the same time, the nonequilibrium structure has a strong influence on the thermomechanical response. Theories for the structural relaxation of glassy materials describe physical aging as a thermodynamic process where the nonequilibrium structure becomes more ordered with time during approach to equilibrium. This produces a decrease in the molecular mobility, which has a significant effect on the stress relaxation time, yield strength, and other physical properties, such as the heat capacity at T_g and even the process of physical aging itself. The effects of structural relaxation are reversed by moderate plastic deformation, which has been hypothesized to increase the disorder of the amorphous structure, thereby increasing the molecular mobility. Experiments have shown that this effect of mechanical rejuvenation saturates at 30% strain at which point the material attains a metastable nonequilibrium state.

In this work, we showed that many characteristics of physical aging and mechanical rejuvenation, observed in the stress-strain response and calorimetry measurements, can be explained by a thermomechanical model that couples structural evolution, as described by an effective temperature distribution, plastic deformation, and a structure-dependent relaxation time [35,36]. Specifically, the Xiao and Nguyen model can predict (1) the increase in the yield strength and the endothermic overshoot in the heat capacity at T_g with the annealing time, (2) the postyield stress drop up to 15% plastic strain, (3) the same draw stress, regardless of the previous thermal history, (4) the decrease in the yield peak stress and endothermic overshoot in the heat capacity at T_g with plastic deformation, (5) the erasure of those features at 15% plastic strain, (6) the appearance of a pre-T_g exothermic undershoot in the heat capacity, where the magnitude of the undershoot increases with the plastic deformation up to 30% strain, (7) the high fraction of stored energy, which is around 45% at 30% strain, and (8) a large fraction of applied work stored in the configurational subsystems at the early stage of the deformation.

The main discrepancy of the model is the occurrence of the exothermic undershoot at a lower temperature than observed in experiments. This appears to suggest the need to incorporate a dependence of the structural relaxation time on the flow stress [43] and the molecular orientation, which is also responsible for strain hardening. The experimental data of Hasan and Boyce [1] showed that another exothermic undershoot in the heat capacity appeared around T_g when polymers were deformed to around or above 60% strain. The current model is not able to capture this phenomena and again shows the necessity of incorporating molecular orientation, which will be a subject of future work.

The Xiao and Nguyen [35] theory shares many similarities with the theories of Buckley and co-workers (e.g., [33,44]) and STZ theories of Langer and co-workers [30]. The theories of Buckley and co-workers do not strictly adhere to a two-temperature thermodynamic framework. Thus, thermodynamic properties such as the internal energy, entropy, and their dependence are not specified. A variety of different phenomenological constitutive relations were proposed for the dependence of the effective temperature on the plastic strain or the rate of change of the effective temperature on the rate of plastic deformation. The STZ theories of Langer and co-workers connect the effective temperature to microstructural defects and derive constitutive relations for the plastic flow and effective temperature based on considerations of STZ dynamics. The Xiao and Nguyen theory is not based on a lower-scale model for the motion of microstructural defects. Rather, we chose phenomenological models with parameters, that for the most part can be measured independently, for the internal energy, configurational entropy, and the temperature and structure dependence of the relaxation times, the dependence of relaxation times on stress, temperature, and structure. This approach has hereby demonstrated good predictive abilities for a wide range of nonequilibrium properties for moderate plastic strain before the onset of significant orientation hardening.

ACKNOWLEDGMENTS

R.X. acknowledges funding support form the National Natural Science Foundation of China (Grant No. 11502068) and China Postdoctoral Science Foundation Funded Project (Grant No. 2016M600354). T.D.N. acknowledges funding support from the National Science Foundation (Grant No. CMMI-1628974).

[1] O. A. Hasan and M. C. Boyce, Polymer **34**, 5085 (1993).
[2] H. van Melick, L. Govaert, and H. Meijer, Polymer **44**, 3579 (2003).
[3] H. E. H. Meijer and L. E. Govaert, Prog. Polym. Sci. **30**, 915 (2005).
[4] L. C. E. Struik, Polym. Eng. Sci. **17**, 165 (1977).
[5] A. Volynskii, A. Efimov, and N. Bakeev, Polym. Sci. Ser. C **49**, 301 (2007).
[6] J. Choi, A. M. Ortega, R. Xiao, C. M. Yakacki, T. D. Nguyen, C. M. Yakachi, and T. D. Nguyen, Polymer **53**, 2453 (2012).
[7] M. Aboulfaraj, C. G'Sell, D. Mangelinck, and G. B. McKenna, J. Non-Cryst. Solids **172-174**, 615 (1994).
[8] H. G. H. van Melick, L. E. Govaert, B. Raas, W. J. Nauta, and H. E. H. Meijer, Polymer **44**, 1171 (2003).
[9] J. Kierkels, C.-L. Dona, T. Tervoort, and L. Govaert, J. Polym. Sci., Part B: Polym. Phys. **46**, 134 (2008).
[10] I. M. Hodge and G. S. Huvard, Macromolecules **16**, 371 (1983).
[11] A. R. Berens and I. M. Hodge, Macromolecules **15**, 756 (1982).
[12] J. M. Hutchinson, Prog. Polym. Sci. **20**, 703 (1995).
[13] T. V. Tropin, G. Schulz, J. W. Schmelzer, and C. Schick, J. Non-Cryst. Solids **409**, 63 (2015).
[14] G. Liu, D. Zhao, and Y. Zuo, J. Non-Cryst. Solids **417**, 52 (2015).
[15] T. M. Kung and J. C. M. Li, J. Mater. Sci. **22**, 3620 (1987).
[16] S. N. Rudnev, O. B. Salamatina, V. V. Voenniy, and E. F. Oleynik, Colloid Polym. Sci. **269**, 460 (1991).
[17] E. Oleinik, S. Rudnev, S. Shenogin, and O. Salamatina, Macromol. Symp. **98**, 967 (1995).
[18] S. V. Shenogin, G. W. H. Höhne, and E. F. Oleinik, Thermochim. Acta **391**, 13 (2002).
[19] E. Oleinik, S. Rudnev, O. Salamatina, S. Shenogin, M. Kotelyanskii, T. Paramzina, and S. Nazarenko, e-Polymers **6**, 366 (2006).
[20] P. Lin, S. Cheng, and S.-Q. Wang, ACS Macro Lett. **3**, 784 (2014).
[21] A. Q. Tool, J. Am. Ceram. Soc. **29**, 240 (1946).
[22] A. J. Kovacs, J. J. Aklonis, J. M. Hutchinson, and A. R. Ramos, J. Polym. Sci. **17**, 1097 (1979).
[23] J. Möller, I. Gutzow, and J. W. Schmelzer, J. Chem. Phys. **125**, 094505 (2006).
[24] G. W. Scherer, J. Non-Cryst. Solids **123**, 75 (1990).
[25] L. F. Cugliandolo, J. Phys. A **44**, 483001 (2011).
[26] T. Nieuwenhuizen, J. Phys. A **201**, L201 (1998).
[27] M. Semkiv and M. Hütter, J. Non-Equilib. Thermodyn. **41**, 79 (2016).
[28] M. Semkiv, P. D. Anderson, and M. Hütter, Continuum Mech. Thermodyn. **29**, 647 (2017).
[29] E. Bouchbinder and J. S. Langer, Phys. Rev. E **80**, 031132 (2009).

[30] M. L. Falk and J. Langer, Annu. Rev. Condens. Matter Phys. **2**, 353 (2011).
[31] J. S. Langer, Phys. Rev. E **92**, 012318 (2015).
[32] J. S. Langer, Phys. Rev. E **70**, 041502 (2004).
[33] C. P. Buckley, P. J. Dooling, J. Harding, and C. Ruiz, J. Mech. Phys. Solids **52**, 2355 (2004).
[34] H. X. Li and C. P. Buckley, Int. J. Plast. **26**, 1726 (2010).
[35] R. Xiao and T. D. Nguyen, J. Mech. Phys. Solids **82**, 62 (2015).
[36] R. Xiao and T. D. Nguyen, Extrem. Mech. Lett. **8**, 70 (2016).
[37] R. Xiao, J. Choi, N. Lakhera, C. Yakacki, C. Frick, and T. Nguyen, J. Mech. Phys. Solids **61**, 1612 (2013).
[38] S. Reese and S. Govindjee, Mech. Time-Depend. Mater. **1**, 357 (1997).
[39] M. L. Manning, J. S. Langer, and J. M. Carlson, Phys. Rev. E **76**, 056106 (2007).
[40] http://sourceforge.net/projects/tahoe/.
[41] E. M. Arruda, M. C. Boyce, and R. Jayachandran, Mech. Mater. **19**, 193 (1995).
[42] O. Salamatina, S. Rudnev, V. Voenniy, and E. Oleynik, J. Therm. Anal. **38**, 1271 (1992).
[43] E. T. J. Klompen, T. A. P. Engels, L. E. Govaert, and H. E. H. Meijer, Macromolecules **38**, 6997 (2005).
[44] H. Li and C. Buckley, Int. J. Solids Struct. **46**, 1607 (2009).